Supporting Information for

Dynamic Coordination Transformation of Active Site in Single-Atom MoS_2 Catalyst for Boosted Oxygen Evolution Catalysis

Nian Ran[1,2], Youwei Wang[1,2], Erhong Song[1,2], Yao Zhou[4,*] and Jianjun Liu[1,2,3,*]

[1]State Key Laboratory of High Performance Ceramics and Superfine Microstructures, Shanghai Institute of Ceramics, Chinese Academy of Sciences, Shanghai 200050, China

[2]Center of Materials Science and Optoelectronics Engineering, University of Chinese Academy of Sciences, Beijing 100049, China

[3]School of Chemistry and Materials Science, Hangzhou Institute for Advanced Study, University of Chinese Academy of Science, 1 Sub-lane Xiangshan, Hangzhou 310024, China

[4]Advanced Research Institute of Multidisciplinary Science, and School of Chemistry and Chemical Engineering, Beijing Institute of Technology, Beijing 100081, China

[*] Corresponding Email: jliu@mail.sic.ac.cn; zhouyao@bit.edu.cn

Supporting Figures

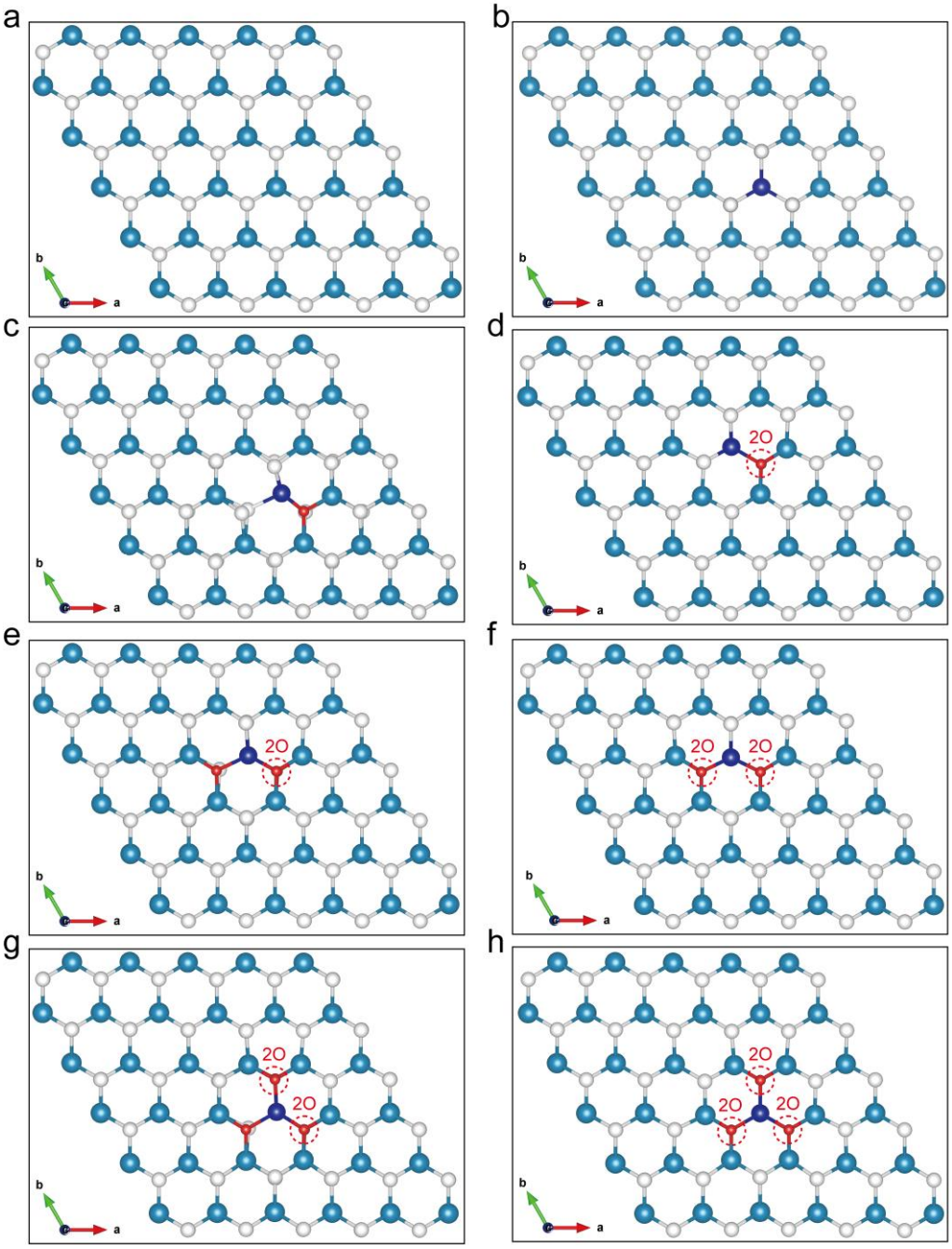

Figure S1. Schematic of transition metal (TM) atom or transition metal atom co-doped with different numbers of oxygen (O) atoms in 2H phase MoS_2. **a,** MoS_2. **b,** TM doped in MoS_2. **c-h,** TM co-doped with 1~6 of O in MoS_2. The white, blue, dark blue, and red colors represent S, Mo, TM, and O atoms, respectively.

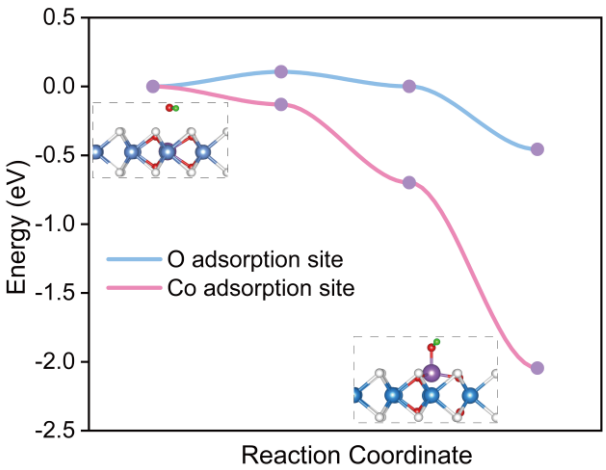

Figure S2. Potential active sites on cobalt co-doped six oxygen atoms in 2H phase MoS_2. The Co site is the active site because it's lower thermodynamic energy and lower potential barrier.

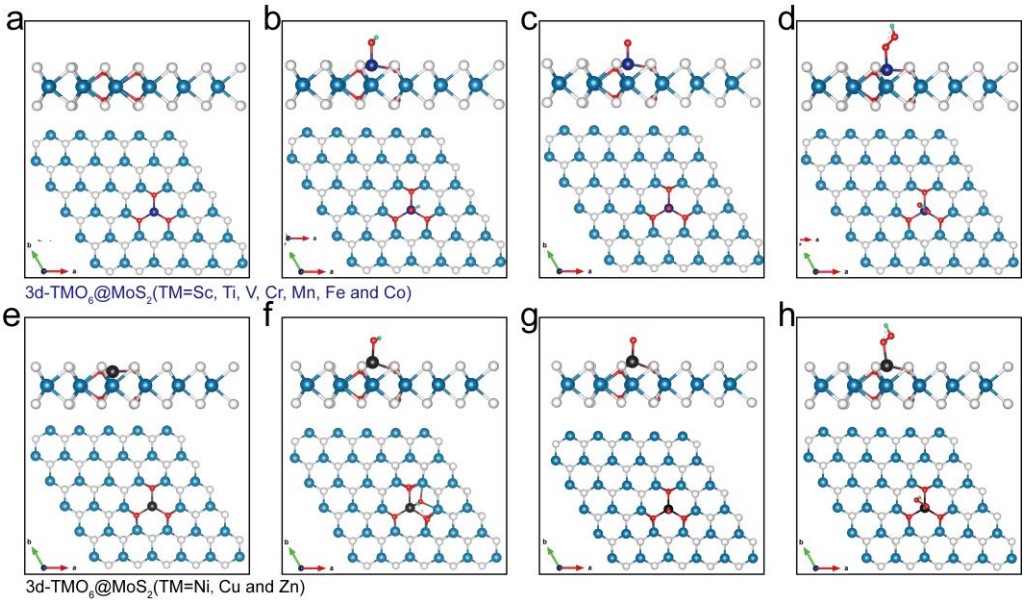

Figure S3. Configurations of adsorbates (O, OH, OOH) on transition metal atom (TM) co-doped with six oxygen atoms in 2H phase MoS_2 with diverse coordination. **a-d,** 3d-TMO_6@MoS_2 (TM=Sc, Ti, V, Cr, Mn, Fe and Co). **e-h,** 3d-TMO_6@MoS_2 (TM=Ni, Cu and Zn). The white, blue, dark blue, dark, green and red colors represent S, Mo, (Sc, Ti, V, Cr, Mn, Fe and Co), (Ni, Cu and Zn), H and O atoms, respectively.

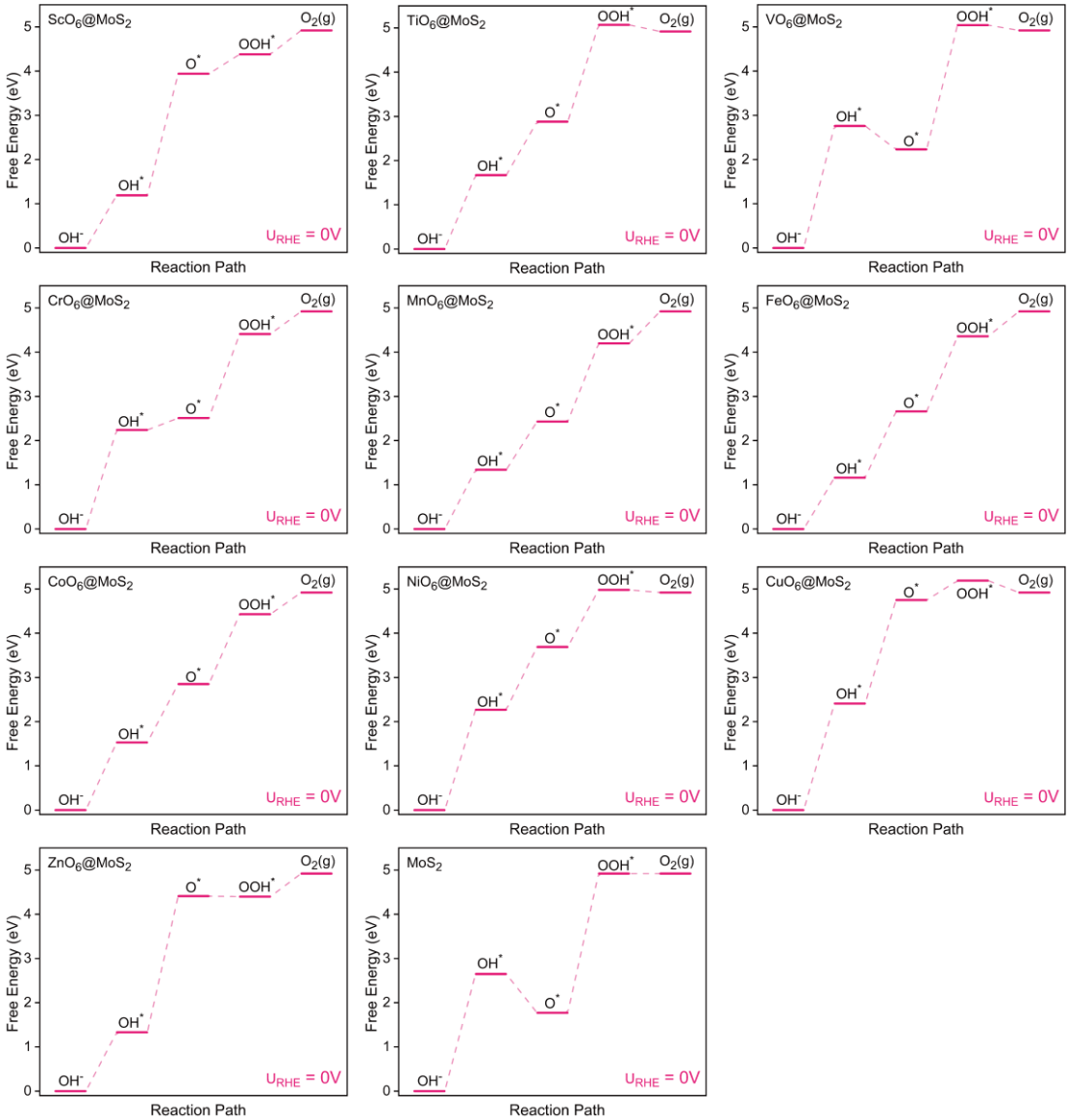

Figure S4. Free-energy diagram for OER on transition metal atom (TM) co-doped with six oxygen atoms in 2H phase MoS_2, at zero electrode potential.

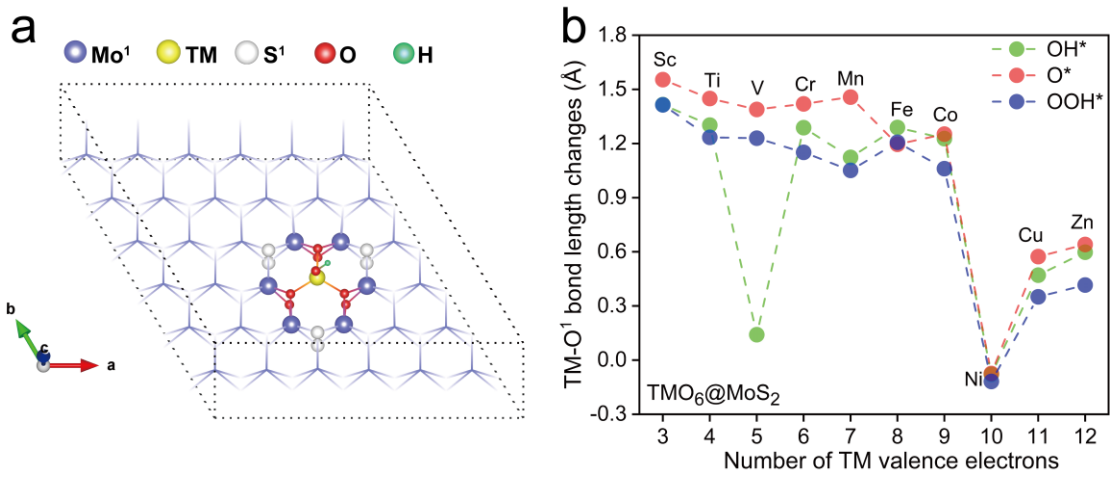

Figure S5. TM-O^1 bond length change after adsorbed OH^*, O^* and OOH^* is an efficient method to determine the movement of active sites. **a,** schematic diagram of the 3d-TMO_6@MoS_2 structure after adsorption of the intermediates (OH*). **b,** the TM-O^1 bond length change of after adsorbed OH^*, O^* and OOH^*, where O^1 represents the oxygen atom on the opposite side of the adsorbed intermediate.

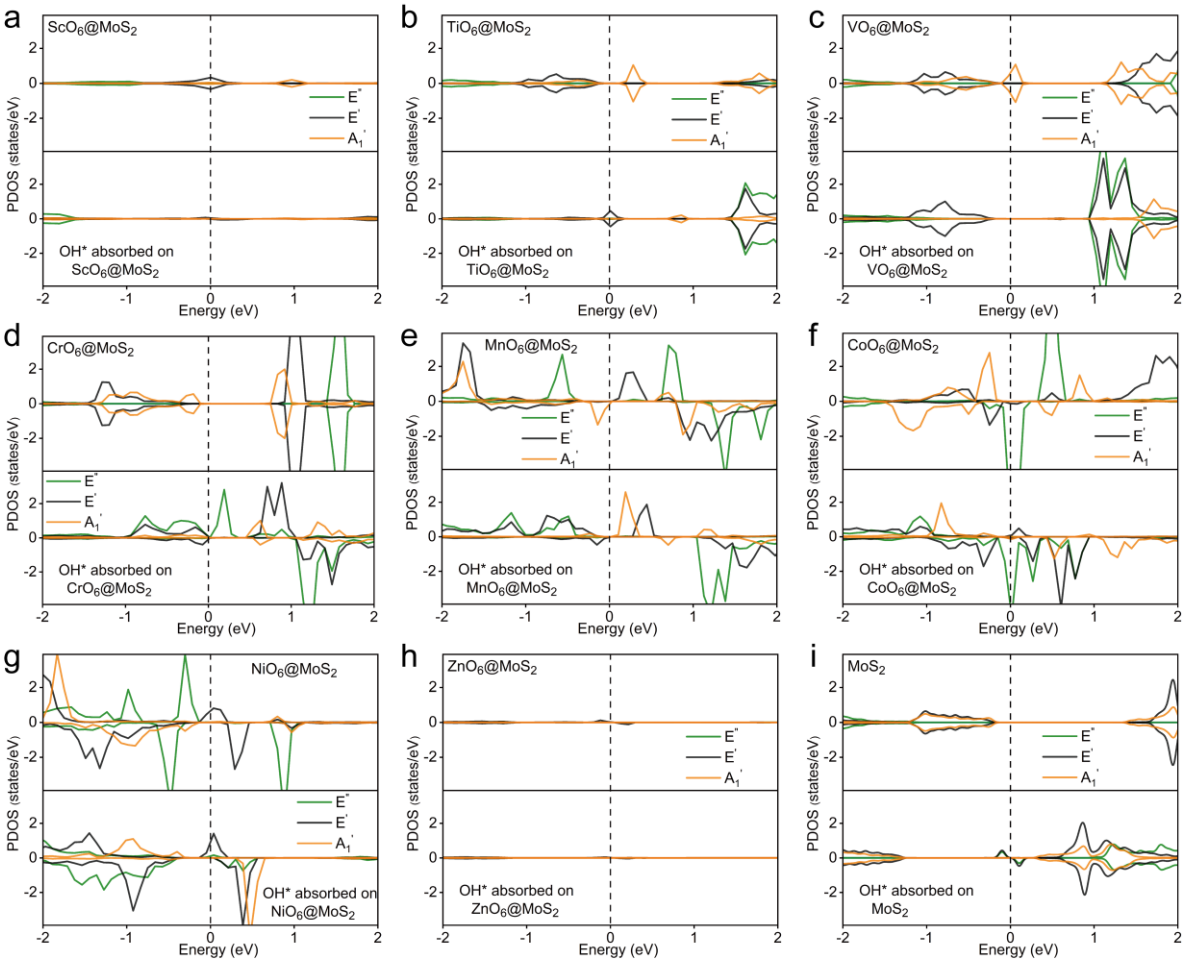

Figure S6. The density of projected states (PDOS) of 3d-TMO_6@MoS_2 and after adsorption OH* on 3d-TMO_6@MoS_2.

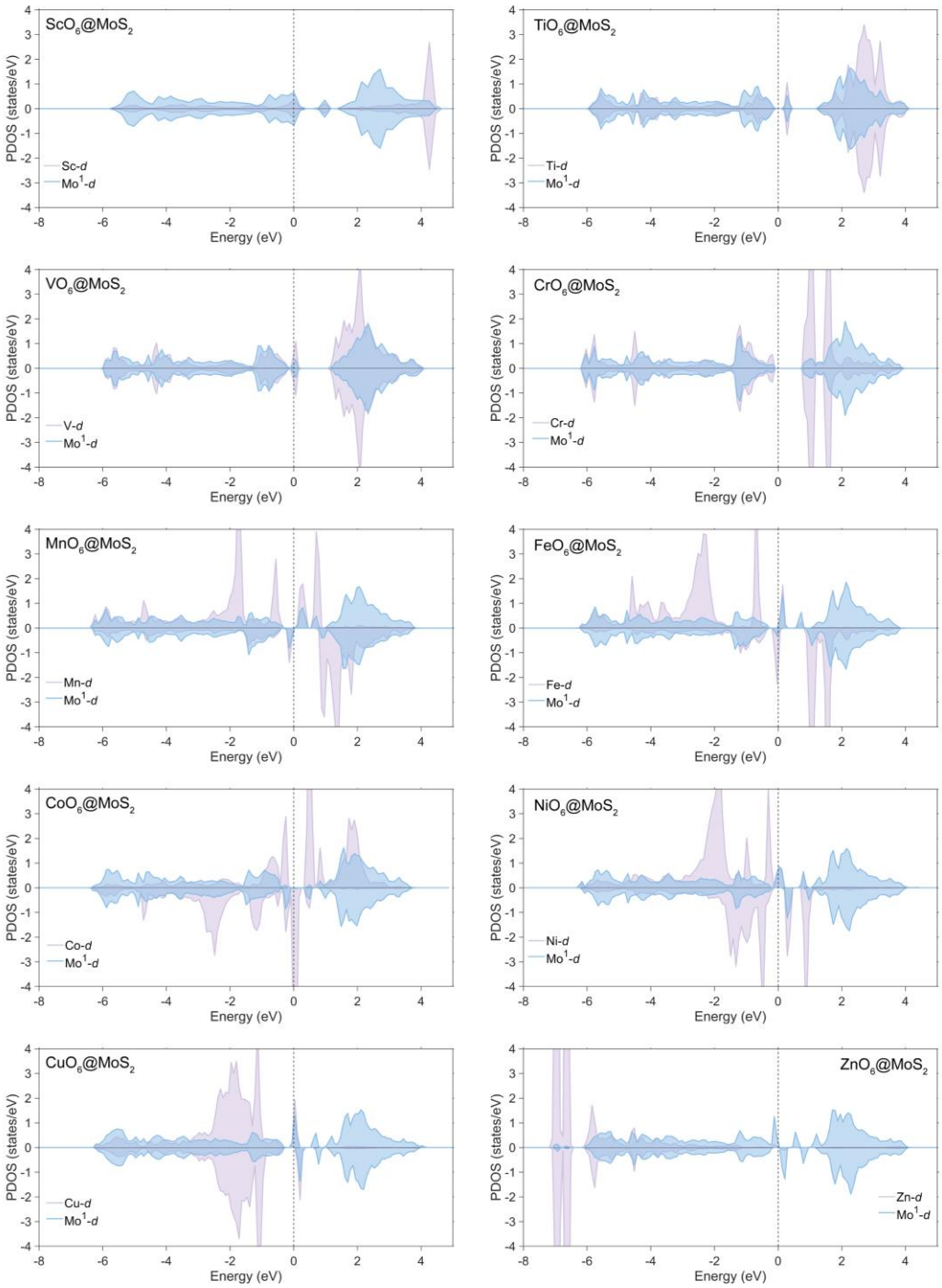

Figure S7. The density of projected states (PDOS) of transition metal atom (TM) co-doped with six oxygen atoms in 2H phase MoS_2, Where Mo^1 represents the nearest neighbor Mo atoms around the doped atoms.

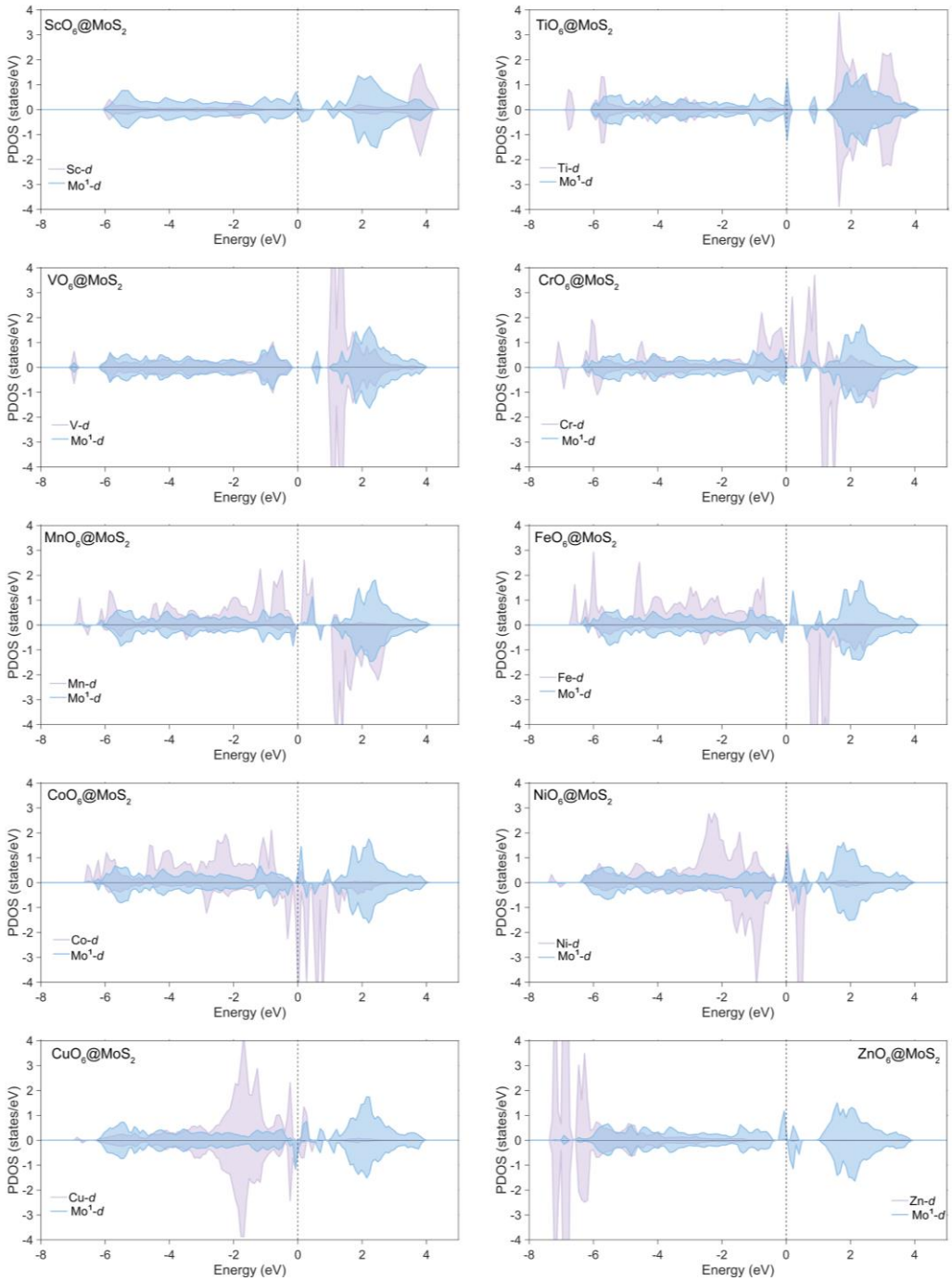

Figure S8. The density of projected states (PDOS) of OH^* on transition metal atom (TM) co-doped with six oxygen atoms in 2H phase MoS_2, Where Mo^1 represents the nearest neighbor Mo atoms around the doped atoms.

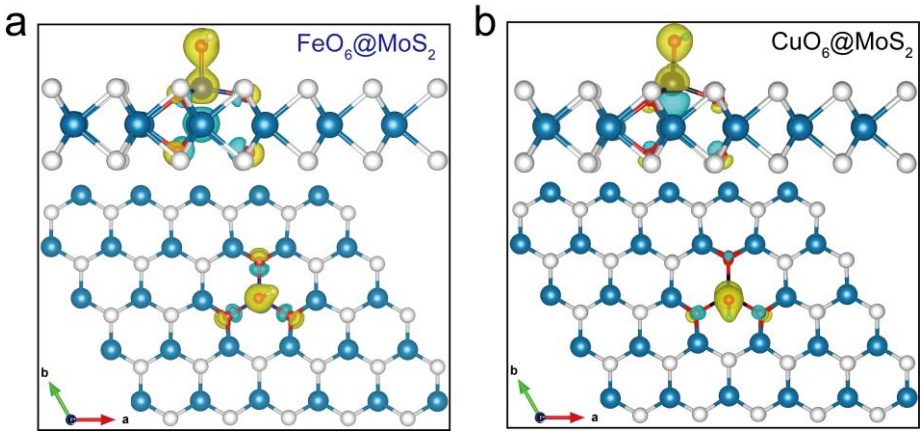

Figure S9. The charge density difference of before adsorption and after desorption on transition metal atom (TM) co-doped with six oxygen atoms in 2H phase MoS_2. **a,** FeO_6@MoS_2. **b,** CuO_6@MoS_2. Yellow and blue represent positive and negative 0.11 e/$Å^3$ isosurfaces, respectively.

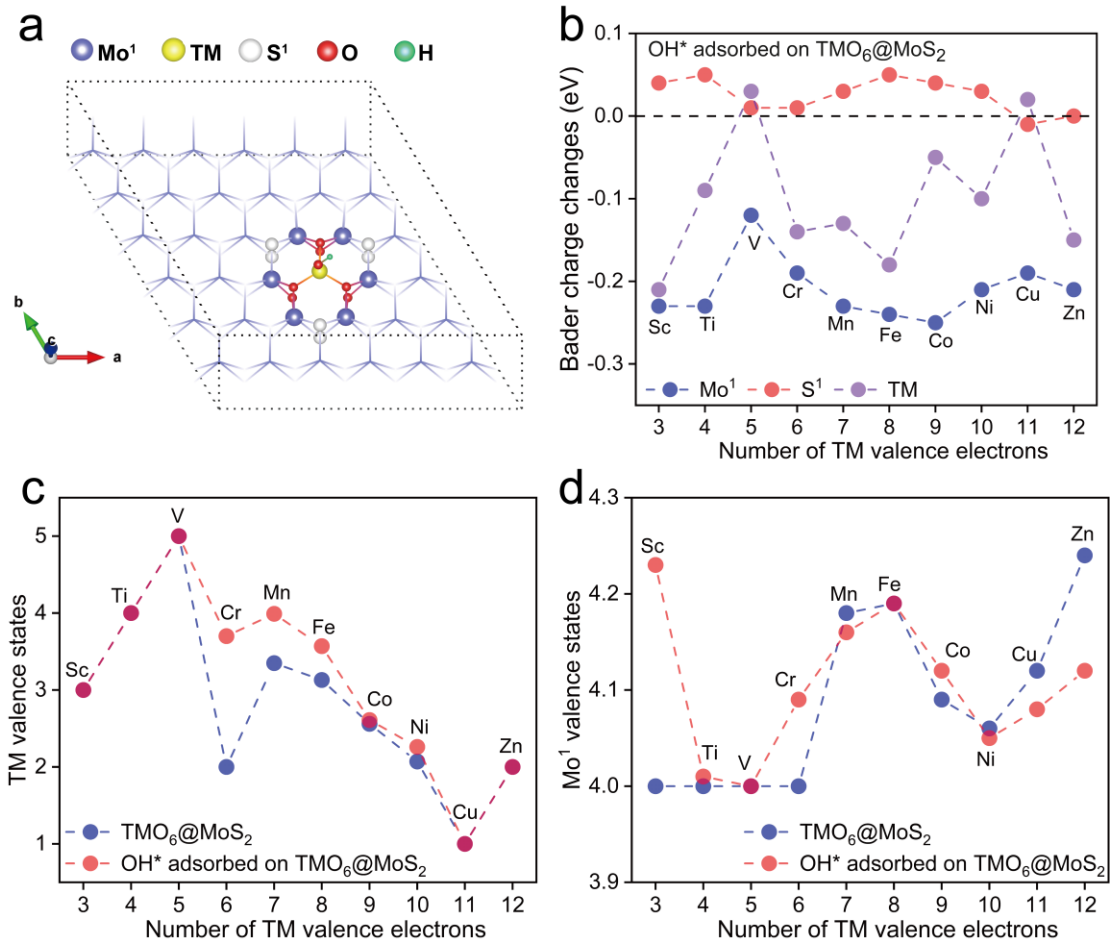

Figure S10. Charge changes of 3d-TMO_6@MoS_2 structure before and after adsorption of OH* intermediate. **a,** schematic diagram of the 3d-TMO_6@MoS_2 structure after adsorption of the OH* intermediate. **b,** Bader charge changes. **c,** TM valence states changes. **d,** Mo^1 valence states changes.

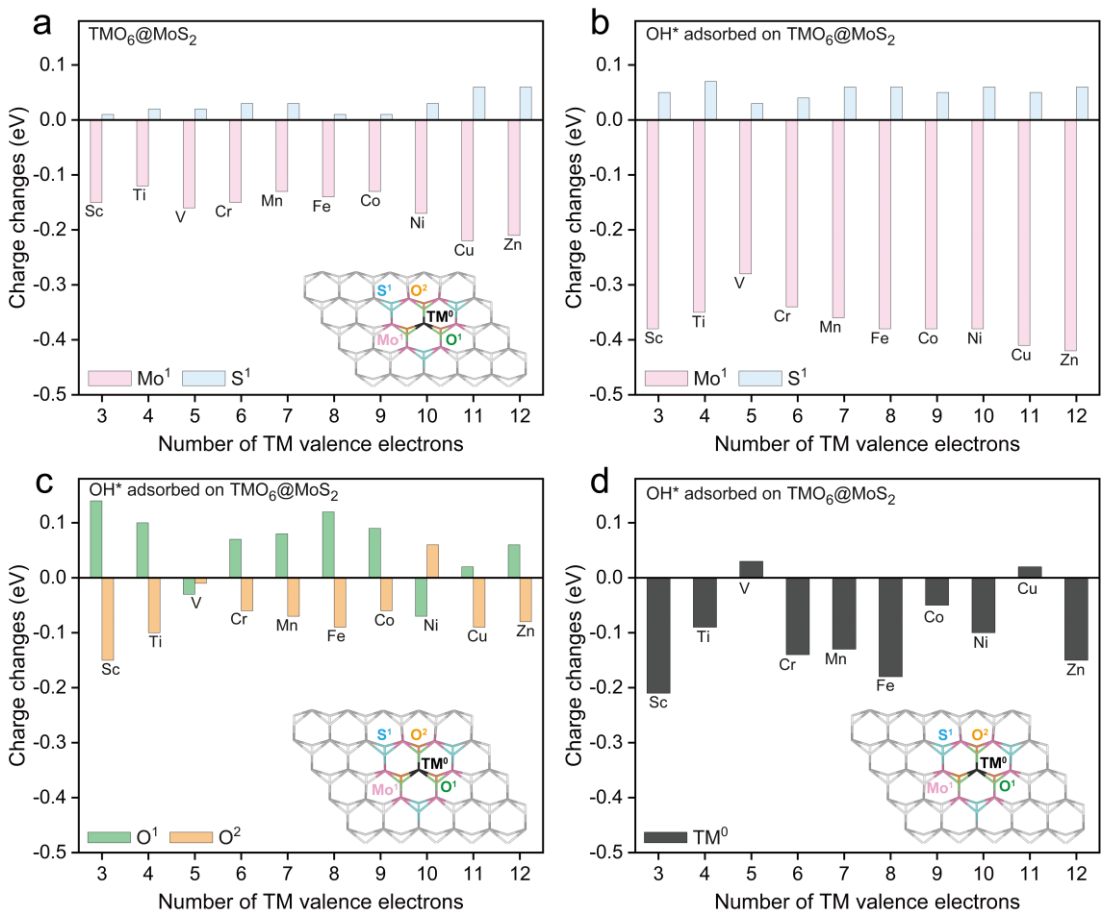

Figure S11. The bader charge of before adsorption and adsorption OH^* on transition metal atom (TM) co-doped with six oxygen atoms in 2H phase MoS_2. **a,** the bader charge of TMO_6@MoS_2 before adsorption. **b-d,** the bader charge of TMO_6@MoS_2 after adsorbed OH^*.

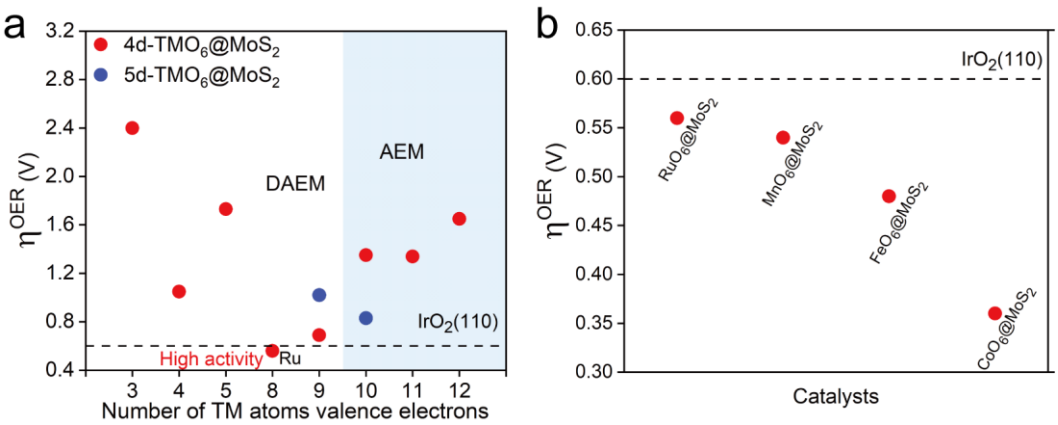

Figure S12. The OER theoretical overpotential on TMO_6@MoS_2. **a,** the theoretical OER overpotential of TMO_6@MoS_2 (including 4d-TM=Y, Zr, Nb, Ru, Rh, Pd, Ag, Cd, Ru and 5d-TM=Ir and Pt). **b,** TMO_6@MoS_2 (TM=Ru, Mn, Fe and Co) with a theoretical OER overpotential below IrO_2(110).

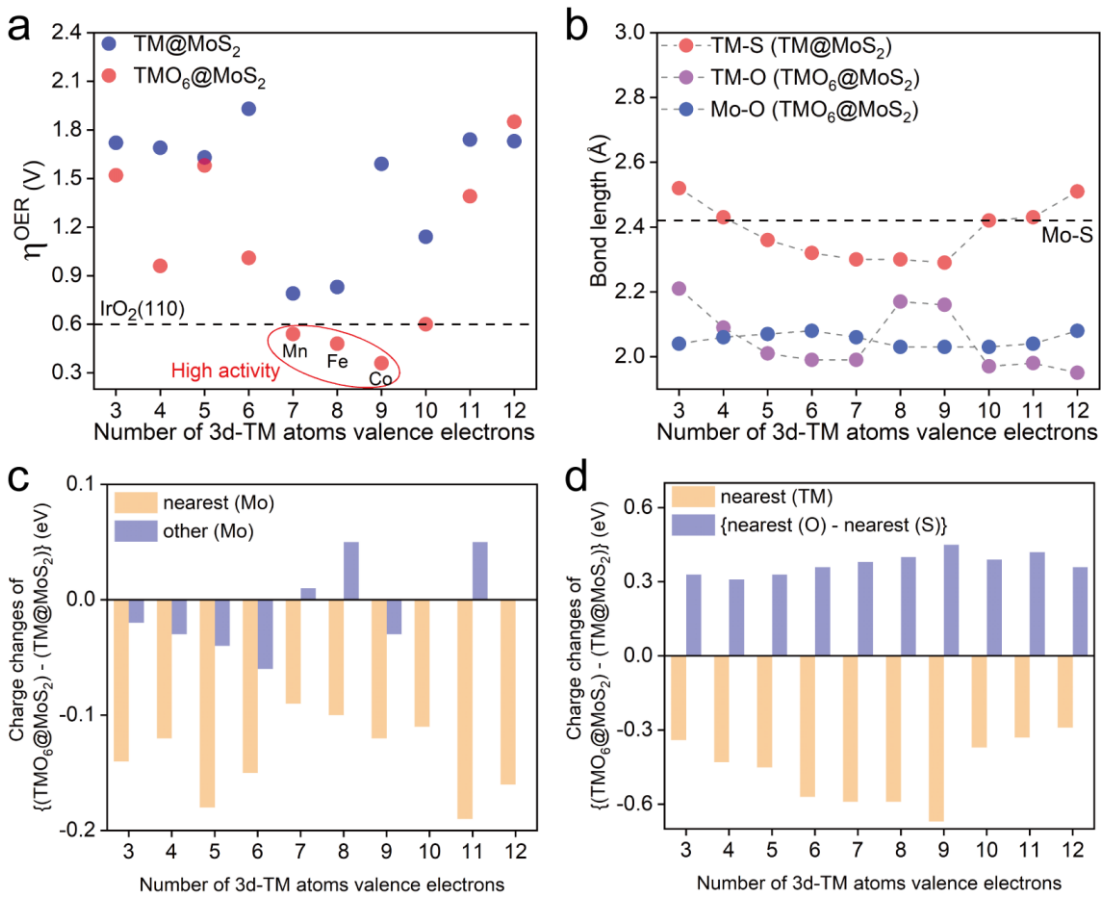

Figure S13. a, the OER theoretical overpotential on $TMO_6@MoS_2$ and $TM@MoS_2$. **b,** the bond length of $TMO_6@MoS_2$ and $TM@MoS_2$. **c,** the charge changes of Mo on $TMO_6@MoS_2$ and $TM@MoS_2$. **d,** the charge changes of TM and {nearest atom(O)-nearest atom(S)} on $TMO_6@MoS_2$ and $TM@MoS_2$.

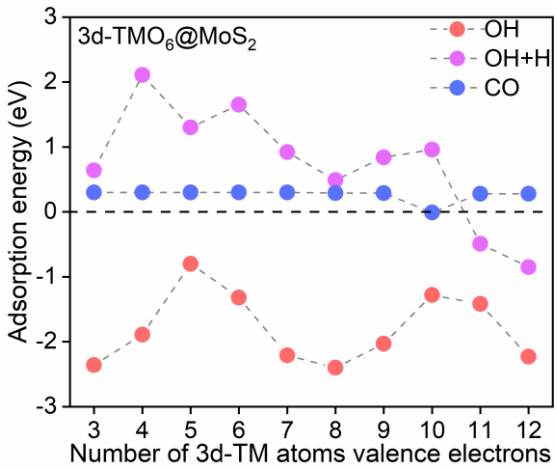

Figure S14. The adsorption energy of CO, OH and OH+H on 3d-TMO_6@MoS_2.

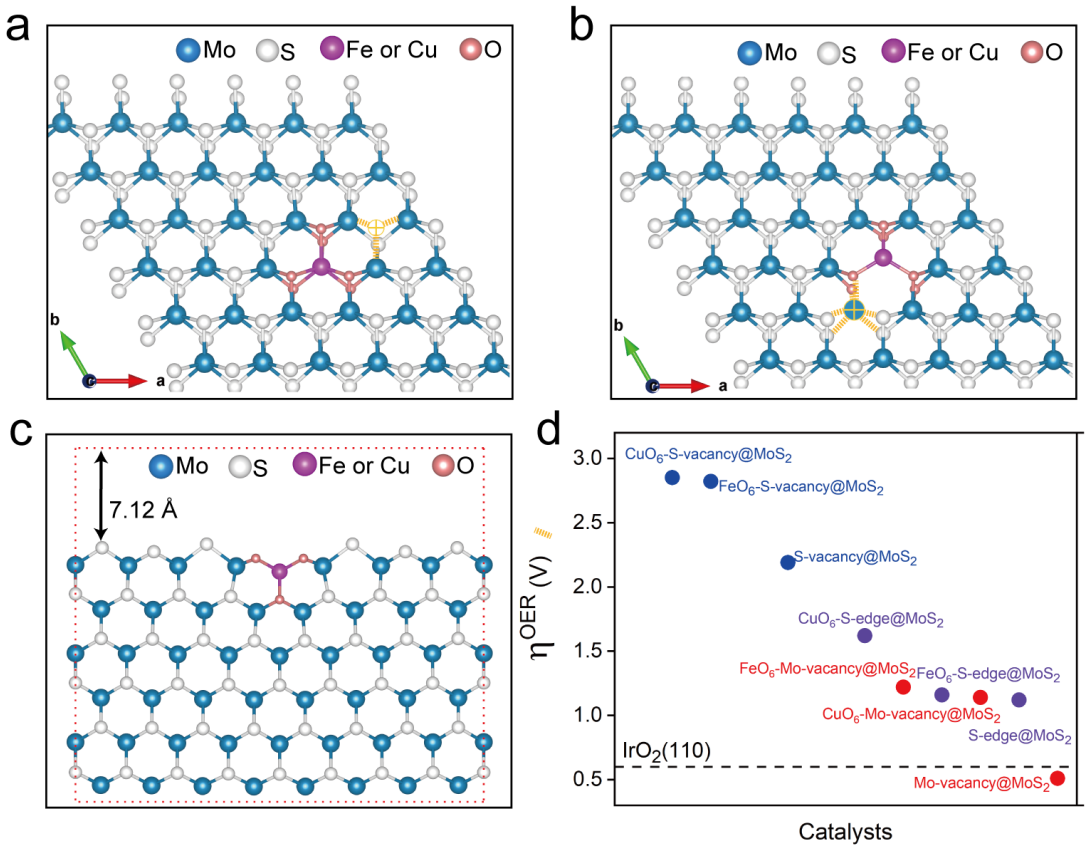

Figure S15. The structure and OER theoretical overpotential of TMO_6@MoS_2 and MoS_2 with different defect structures (S-vacancy, Mo-vacancy, S-edge, Mo-edge). **a,** the structure of TMO_6@MoS_2 with S-vacancy. **b,** the structure of TMO_6@MoS_2 with Mo-vacancy. **c,** the structure of TMO_6@MoS_2 with Mo-edge. **d,** the OER theoretical overpotential of TMO_6@MoS_2 and MoS_2 with different defect structures (S-vacancy, Mo-vacancy, S-edge, Mo-edge).

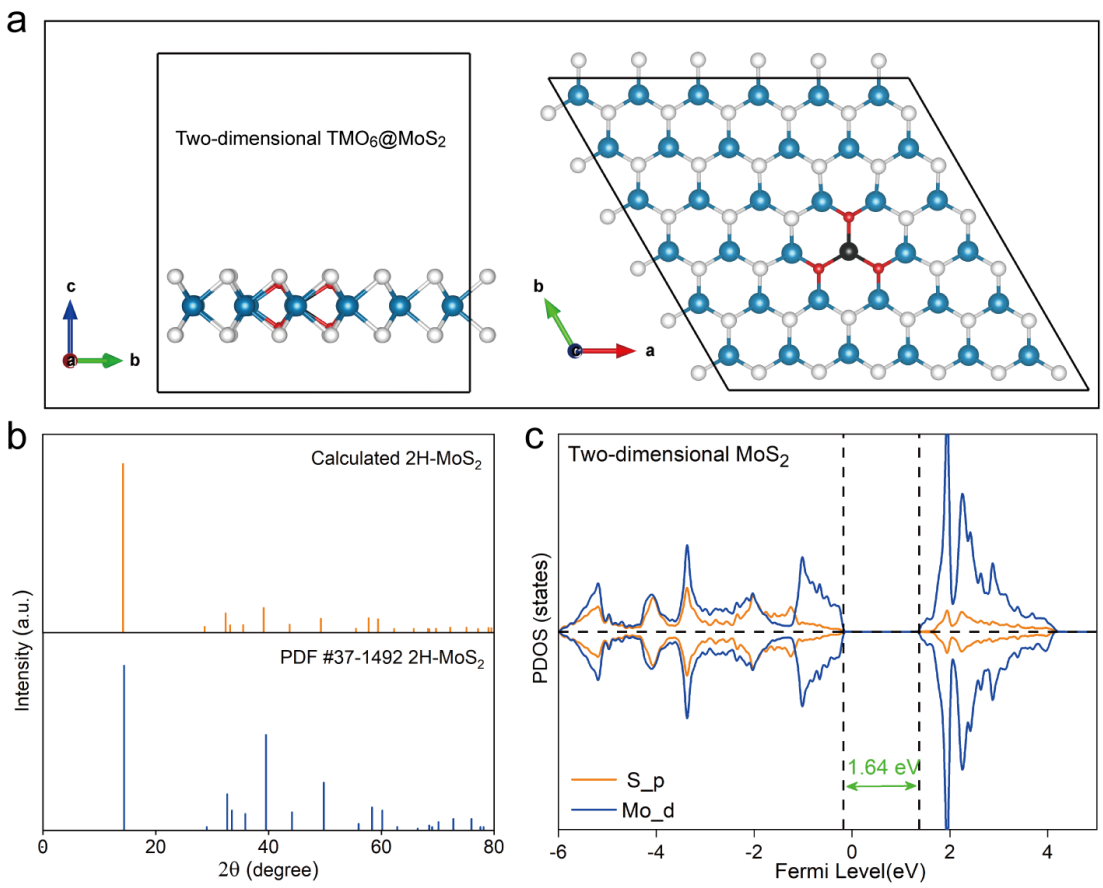

Figure S16. a, Schematic of transition metal atom co-doped with six numbers of oxygen (O) atoms in 2H phase MoS_2. **b,** Comparison between the experimental and calculated XRD patterns of 2H-MoS_2 (space group is $P6_3/mmc$). **c,** The density of projected states (PDOS) of two-dimensional MoS_2.

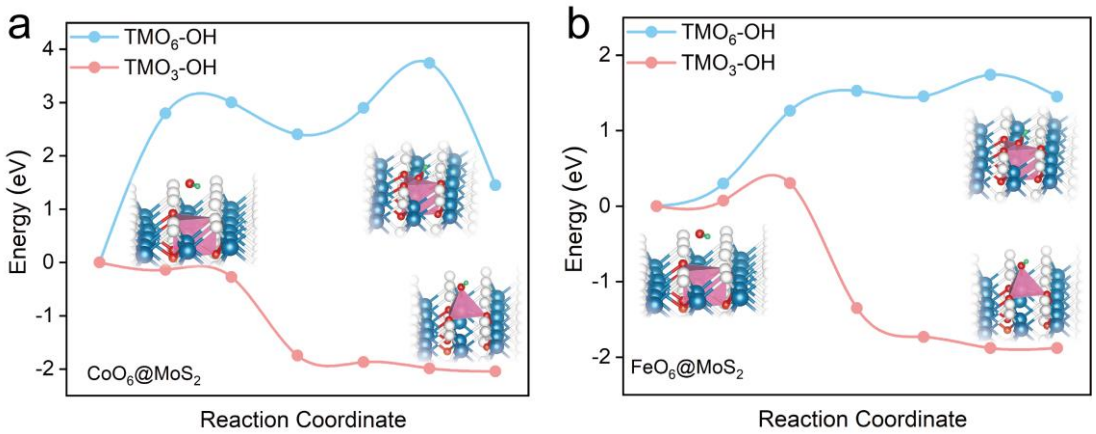

Figure S17. Potential barrier of tetra-coordinated structure (TMO_3-OH) and hexa-coordinated structure (TMO_6-OH) of TM (TM=Co and Fe) co-doped six oxygen atoms in 2H phase MoS_2 during OER reaction. The tetra-coordinated structure (TMO_3-OH) is the active structure because it's lower thermodynamic energy and lower potential barrier.

Supplementary Note 1. *In situ* Raman spectra of FeO_6@MoS_2 and CuO_6@MoS_2

The peaks located at ~405 and ~380 cm^{-1} correspond to the characteristic A_{1g} mode and E_{2g}^1 mode of MoS_2[1]. In addition, the peaks in Figure S18a-b related to A_g-δ(OMo_3) (~337 cm^{-1}), B_{1g}-ν(OMo_3) (~453 and 491 cm^{-1}) confirmed the successful introduction of oxygen into MoS_2 lattice[2]. For sample FeO_6@MoS_2, Raman peak of [FeO_6] at ~636 cm^{-1}[3] gradually decreases and the peak of [FeO_x] (x<5) at ~766 cm^{-1}[4] appears as the applied potential increases to 1.45 V (Figure S18a). The peak at ~566 cm^{-1} (highlighted by gray dashed line) supports the formation of FeOOH* species[5]. For sample CuO_6@MoS_2, Raman peak of [CuO_3] at ~660 cm^{-1}[6] in Figure S18b shows no change during OER process, and the CuOOH* species[7] (highlighted by gray dashed line) appears when applied potential is no less than 1.65 V. These results are consistent with the theoretical predictions (Figure 3c-d).

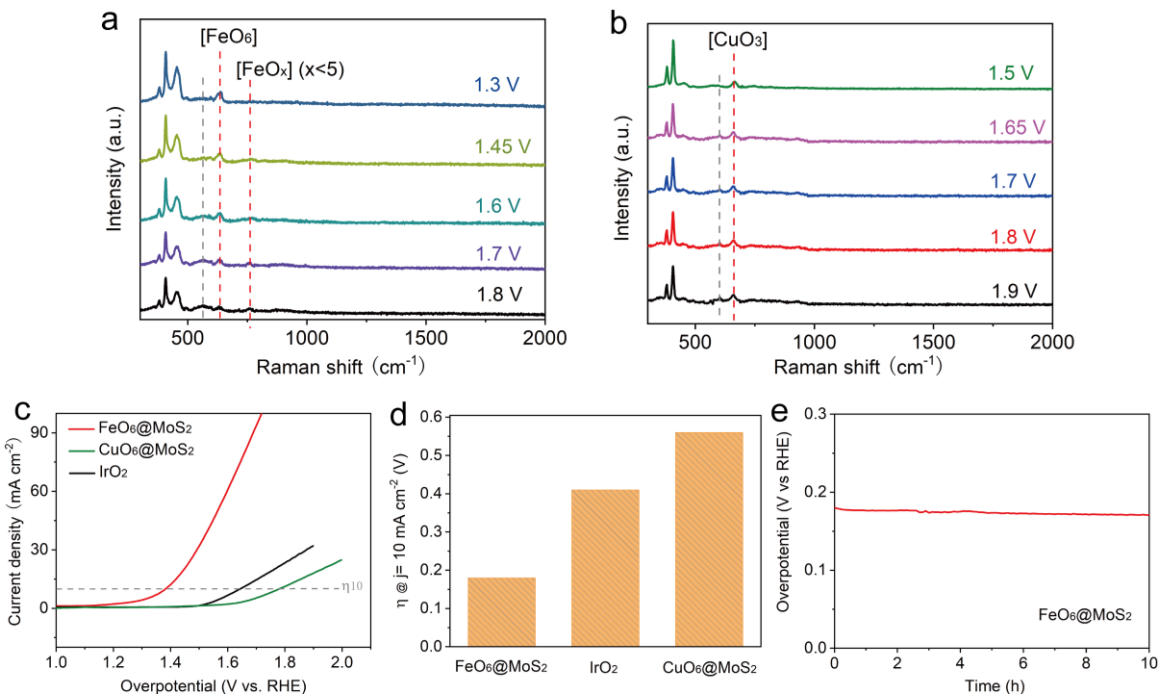

Figure S18. **a-b**, In-situ Raman spectra of the CuO_6@MoS_2 and FeO_6@MoS_2, respectively. **c**, LSV curves and **d,** η_{10} values of as-prepared samples CuO_6@MoS_2, FeO_6@MoS_2, and IrO_2. **e**, Long-term OER stability of the FeO_6@MoS_2 sample at a constant current of 10 mA cm^{-2}.

Supporting Tables

Table S1. The bond length of Mo-S in MoS_2 and TM-O in $LiTMO_2$.

Material systems	Bond	Bond length (Å)
MoS_2	Mo-S	2.40
$LiCoO_2$	Co-O	1.94
$LiFeO_2$	Fe-O	2.05
$LiMnO_2$	Mn-O	1.96/ 2.34
$LiTiO_2$	Ti-O	2.04/ 2.12
$LiNiO_2$	Ni-O	1.91
$LiVO_2$	V-O	2.06
$LiCrO_2$	Cr-O	2.03
$LiZrO_2$	Zr-O	2.18
$LiNbO_2$	Nb-O	2.16
$LiRuO_2$	Ru-O	2.09
$LiRhO_2$	Rh-O	2.09

Table S2. Binding energy of MoO_X and MoS_X with different numbers of oxygen/ sulfur atoms doped in 2H phase MoS_2.

Material systems	MoO_X binding energy (eV)	MoS_X binding energy (eV)
O_1@MoS_2	-7.47	-6.31
O_2@MoS_2	-7.43	-6.07
O_3@MoS_2	-7.41	-6.19
O_4@MoS_2	-7.48	-6.23
O_5@MoS_2	-7.44	-6.27
O_6@MoS_2	-7.52	-6.16

Table S3. The formation energy (E_F) of transition metal atom (TM) doped in 2H phase MoS_2.

Material systems	ΔE_F (eV)
Sc@MoS_2	-0.18
Ti@MoS_2	-2.06
V@MoS_2	-4.02
Cr@MoS_2	-5.29
Mn@MoS_2	-4.65
Fe@MoS_2	-3.11
Co@MoS_2	-1.08
Ni@MoS_2	0.99
Cu@MoS_2	5.71
Zn@MoS_2	9.64
MoS_2	-0.69

Table S4. The formation energy (E_F) of transition metal atom (TM) co-doped with six oxygen atoms in 2H phase MoS_2.

Material systems	ΔE_F (eV)
ScO_6@MoS_2	-3.91
TiO_6@MoS_2	-2.50
VO_6@MoS_2	-3.03
CrO_6@MoS_2	-3.33
MnO_6@MoS_2	-2.14
FeO_6@MoS_2	-3.00
CoO_6@MoS_2	-2.75
NiO_6@MoS_2	-2.73
CuO_6@MoS_2	-4.63
ZnO_6@MoS_2	-4.93
MoS_2	-0.69

Table S5. The energy of TM atom moving from the triangular prism crystal field to the triangular pyramid crystal field in $TMO_6@MoS_2$.

Material systems	Energy (eV)
$ScO_6@MoS_2$	0.09
$TiO_6@MoS_2$	0.01
$VO_6@MoS_2$	0.01
$CrO_6@MoS_2$	1.75
$MnO_6@MoS_2$	0.02
$FeO_6@MoS_2$	0.54
$CoO_6@MoS_2$	0.77
$NiO_6@MoS_2$	-0.22
$CuO_6@MoS_2$	-0.49
$ZnO_6@MoS_2$	-0.47
$O_6@MoS_2$	4.49
MoS_2	7.99

Table S6. In $TMO_6@MoS_2$, when OH* is adsorbed and O2 is desorbed respectively, the energy difference of TM atom (the triangular prism crystal field is subtracted from the triangular pyramid crystal field).

Material systems	Energy (OH*) (eV)	Energy (O_2) (eV)
$ScO_6@MoS_2$	-1.52	0.34
$TiO_6@MoS_2$	-1.00	0.84
$VO_6@MoS_2$	-0.91	1.16
$CrO_6@MoS_2$	-0.59	1.11
$MnO_6@MoS_2$	-0.89	-0.23
$FeO_6@MoS_2$	-0.17	0.61
$CoO_6@MoS_2$	-0.90	-0.92
$NiO_6@MoS_2$	-0.79	-0.31
$CuO_6@MoS_2$	-0.99	-0.49
$ZnO_6@MoS_2$	-1.55	-0.20
$O_6@MoS_2$	0.35	1.95
MoS_2	1.72	5.37

Table S7. Adsorption free energies of OH^*, O^*, OOH^*, H^* (eV) on Pt (111), IrO_2 and RuO_2.

Active site	ΔG_{OH}^*	ΔG_{O}^*	ΔG_{OOH}^*	ΔG_{H}^*
Pt (111)	/	/	/	-0.09
IrO_2 (110)	0.19	1.34	3.09	/
RuO_2 (110)	0.15	1.62	3.31	/

Table S8. Theoretical overpotential for OER (η^{OER}, V vs RHE), theoretical overpotential (η^{HER}, V vs RHE) for HER on Pt (111), IrO_2 and RuO_2.

Active site	η^{OER}	η^{HER}
Pt (111)	/	-0.09
IrO_2 (110)	0.60	/
RuO_2 (110)	0.47	/

Table S9. Adsorption free energies of OH^*, O^*, OOH^* (eV) on transition metal atom doped in 2H phase MoS_2.

Material systems	ΔG_{OH}^*	ΔG_{O}^*	ΔG_{OOH}^*
Sc@MoS_2	1.21	1.68	4.63
Ti@MoS_2	1.25	1.71	4.63
V@MoS_2	1.19	1.70	4.56
Cr@MoS_2	2.36	1.63	4.79
Mn@MoS_2	1.84	1.57	3.59
Fe@MoS_2	1.62	1.50	3.56
Co@MoS_2	0.80	1.48	4.30
Ni@MoS_2	0.35	1.47	3.84
Cu@MoS_2	0.64	1.15	4.12
Zn@MoS_2	0.89	1.39	4.35
MoS_2	2.65	1.77	4.92

Table S10. Adsorption free energies of OH^*, O^*, OOH^* (eV) on transition metal atom (TM) co-doped with six oxygen atoms in 2H phase MoS_2.

Material systems	ΔG_{OH}^*	ΔG_O^*	ΔG_{OOH}^*
$ScO_6@MoS_2$	1.19	3.94	4.38
$TiO_6@MoS_2$	1.67	2.88	5.07
$VO_6@MoS_2$	2.76	2.23	5.04
$CrO_6@MoS_2$	2.24	2.51	4.41
$MnO_6@MoS_2$	1.34	2.43	4.20
$FeO_6@MoS_2$	1.16	2.66	4.36
$CoO_6@MoS_2$	1.53	2.85	4.43
$NiO_6@MoS_2$	1.83	3.37	4.70
$CuO_6@MoS_2$	2.14	4.75	5.19
$ZnO_6@MoS_2$	1.33	4.41	4.40
MoS_2	2.65	1.77	4.92

Table S11. Theoretical overpotential for OER (η^{OER}, V vs RHE) on transition metal atom in 2H phase MoS_2. The catalytic performance better than or comparable to IrO_2 is marked with red.

Material systems	η^{OER}	η^{HER}
$Sc@MoS_2$	1.72	-0.21
$Ti@MoS_2$	1.69	-0.31
$V@MoS_2$	1.63	-0.49
$Cr@MoS_2$	1.93	-1.16
$Mn@MoS_2$	0.79	-0.71
$Fe@MoS_2$	0.83	-0.43
$Co@MoS_2$	1.59	-0.16
$Ni@MoS_2$	1.14	-0.56
$Cu@MoS_2$	1.74	-0.45
$Zn@MoS_2$	1.73	-0.24
MoS_2	1.92	-2.02

Table S12. Theoretical overpotential for OER (η^{OER}, V vs RHE) on transition metal atom (TM) co-doped with six oxygen atoms in 2H phase MoS_2. The catalytic performance better than or comparable to IrO_2 is marked with red.

Material systems	η^{OER}
ScO_6@MoS_2	1.52
TiO_6@MoS_2	0.96
VO_6@MoS_2	1.58
CrO_6@MoS_2	1.01
MnO_6@MoS_2	0.54
FeO_6@MoS_2	0.48
CoO_6@MoS_2	0.36
NiO_6@MoS_2	0.60
CuO_6@MoS_2	1.39
ZnO_6@MoS_2	1.85
MoS_2	1.92

Table S13. The overpotential (η^{OER}) for oxygen evolution of experimental (measured at 1M KOH electrolyte and a current density of 10 mA/cm^2) value and calculated value in this paper.

Catalyst	Current density (mA/cm^2)	Experimental η^{OER}(V)	DFT η^{OER}(V)	Refs
Ni@MoS_2	10	0.365	1.14	8
MoS_2	10	0.403	1.92	9
Co@MoS_2	10	0.294	1.59	9
Fe@MoS_2	50	0.290	0.83	10
Co@MoS_2	10	0.260	1.59	11
MoS_2	10	0.420	1.92	11
Co@MoS_2	10	0.270	1.59	12
MoS_2	10	0.392	1.92	12
IrO_2	10	0.314	0.60	13
RuO_2	10	0.210	0.47	11
IrO2	10	0.468	0.60	14
NiVIr-LDH	10	0.18		15
$Ni_{0.75}V_{0.25}$-LDH	10	0.31		16
$Ni_{0.75}Fe_{0.25}$-LDH	10	0.25		16
NiFeMn-LDH	10	0.262		17

$Ni_3Fe_{0.5}V_{0.5}$-LDH	10	0.20		[18]
NiFe-LDH	10	0.36		[19]
NiFe-LDH	10	0.329		[20]
TiNiFe-LDH	10	0.307		[20]
VNiFe-LDH	10	0.287		[20]
CrNiFe-LDH	10	0.295		[20]
MnNiFe-LDH	10	0.313		[20]
CoNiFe-LDH	10	0.290		[20]
CuNiFe-LDH	10	0.317		[20]
ZnNiFe-LDH	10	0.325		[20]
MgNiFe-LDH	10	0.372		[20]
AlNiFe-LDH	10	0.374		[20]
Ni@MoS_2	10	1.08	1.14	[21]
Fe@MoS_2	10	1.10	0.83	[10]

Table S14. O^2-TM bond length changes on transition metal atom (TM) co-doped with six oxygen atoms in 2H phase MoS_2, Where B^1 represents the bond length of O^2-TM, B^2 represents the bond length of O^2-TM after adsorbed OH^*, B^3 represents the bond length of O^2-TM after adsorbed O^*, B^4 represents the bond length of O^2-TM after adsorbed OOH^*, B^5 represents the bond length of O^2-TM after desorbed.

Material systems	B^1	B^2	B^3	B^4	B^5
ScO_6@MoS_2	2.20	3.62	3.76	3.62	2.21
TiO_6@MoS_2	2.09	3.39	3.53	3.32	2.08
VO_6@MoS_2	2.02	2.16	3.41	3.25	3.05
CrO_6@MoS_2	1.99	3.28	3.41	3.14	1.99
MnO_6@MoS_2	2.06	3.18	3.52	3.11	2.49
FeO_6@MoS_2	2.14	3.43	3.34	3.35	2.17
CoO_6@MoS_2	2.18	3.40	3.43	3.24	2.82
NiO_6@MoS_2	2.07	1.99	2.00	1.95	1.95
CuO_6@MoS_2	3.03	3.50	3.60	3.38	3.04
ZnO_6@MoS_2	3.12	3.72	3.76	3.54	3.13

Table S15. The atomic magnetic moment of on transition metal atom (TM) co-doped with six oxygen atoms in 2H phase MoS_2 before adsorption, including nearest neighbor

Mo atoms (Mo^1), O on the same side of OH adsorbent (O^1), O on the opposite side of OH^* adsorbent (O^2) and transition metal atom (TM).

Material systems	Mo^1	O^1	O^2	TM
ScO_6@MoS_2	0.00	0.00	0.00	0.00
TiO_6@MoS_2	0.00	0.00	0.00	0.00
VO_6@MoS_2	0.00	0.00	0.00	0.00
CrO_6@MoS_2	0.00	0.00	0.00	0.00
MnO_6@MoS_2	0.18	0.01	0.03	2.35
FeO_6@MoS_2	0.19	0.04	0.04	3.13
CoO_6@MoS_2	0.09	0.02	0.03	2.44
NiO_6@MoS_2	0.06	0.06	0.06	1.07
CuO_6@MoS_2	0.12	0.02	0.00	0.14
ZnO_6@MoS_2	0.24	0.02	0.01	0.02

Table S16. The atomic magnetic moment of on transition metal atom (TM) co-doped with six oxygen atoms in 2H phase MoS_2 after desorption, including nearest neighbor Mo atoms (Mo^1), O on the same side of OH adsorbent (O^1), O on the opposite side of OH^* adsorbent (O^2) and transition metal atom (TM).

Material systems	Mo^1	O^1	O^2	TM
ScO_6@MoS_2	0.23	0.00	0.02	0.02
TiO_6@MoS_2	0.01	0.00	0.00	0.00
VO_6@MoS_2	0.00	0.00	0.00	0.00
CrO_6@MoS_2	0.09	0.02	0.01	1.70
MnO_6@MoS_2	0.16	0.01	0.01	2.99
FeO_6@MoS_2	0.19	0.07	0.02	3.57
CoO_6@MoS_2	0.12	0.07	0.01	2.39
NiO_6@MoS_2	0.05	0.07	0.07	1.26
CuO_6@MoS_2	0.08	0.07	0.02	0.05
ZnO_6@MoS_2	0.12	0.04	0.02	0.01

Table S17. The valence state of on transition metal atom (TM) co-doped with six oxygen atoms in 2H phase MoS_2 before adsorption, including nearest neighbor Mo

atoms (Mo^1), O on the same side of OH adsorbent (O^1), O on the opposite side of OH^* adsorbent (O^2) and transition metal atom (TM).

Material systems	Mo^1	O^1	O^2	TM
$ScO_6@MoS_2$	+4	-2	-2	+3
$TiO_6@MoS_2$	+4	-2	-2	+4
$VO_6@MoS_2$	+4	-2	-2	+5
$CrO_6@MoS_2$	+4	-2	-2	+2
$MnO_6@MoS_2$	+4.18	-2	-2	+3.35
$FeO_6@MoS_2$	+4.19	-2	-2	+3.13
$CoO_6@MoS_2$	+4.09	-2	-2	+2.56
$NiO_6@MoS_2$	+4.06	-2	-2	+2.07
$CuO_6@MoS_2$	+4.12	-2	-2	+1
$ZnO_6@MoS_2$	+4.24	-2	-2	+2

Table S18. The valence state of on transition metal atom (TM) co-doped with six oxygen atoms in 2H phase MoS_2 after desorption, including nearest neighbor Mo atoms (Mo^1), O on the same side of OH adsorbent (O^1), O on the opposite side of OH^* adsorbent (O^2) and transition metal atom (TM).

Material systems	Mo^1	O^1	O^2	TM
$ScO_6@MoS_2$	+4.23	-2	-2	+3
$TiO_6@MoS_2$	+4.01	-2	-2	+4
$VO_6@MoS_2$	+4	-2	-2	+5
$CrO_6@MoS_2$	+4.09	-2	-2	+3.7
$MnO_6@MoS_2$	+4.16	-2	-2	+3.99
$FeO_6@MoS_2$	+4.19	-2	-2	+3.57
$CoO_6@MoS_2$	+4.12	-2	-2	+2.61
$NiO_6@MoS_2$	+4.05	-2	-2	+2.26
$CuO_6@MoS_2$	+4.08	-2	-2	+1
$ZnO_6@MoS_2$	+4.12	-2	-2	+2

Table S19. The bader charge of transition metal atom (TM) co-doped with six oxygen atoms in 2H phase MoS_2, including nearest neighbor Mo atoms (Mo^1), other Mo atoms

(Mo^2), nearest neighbor S atoms (S^1), other S atoms (S^2), O atom (O^0) and transition metal atom (TM).

Material systems	Mo^1	Mo^2	S^1	S^2	O^0	TM
ScO_6@MoS_2	4.87	5.02	6.49	6.48	6.92	9.17
TiO_6@MoS_2	4.90	5.02	6.49	6.47	6.88	2.27
VO_6@MoS_2	4.85	5.01	6.50	6.48	6.86	3.41
CrO_6@MoS_2	4.85	5.00	6.51	6.48	6.85	4.54
MnO_6@MoS_2	4.88	5.01	6.50	6.47	6.85	5.67
FeO_6@MoS_2	4.87	5.01	6.48	6.47	6.86	6.74
CoO_6@MoS_2	4.89	5.02	6.48	6.47	6.83	7.86
NiO_6@MoS_2	4.84	5.01	6.50	6.47	6.84	9.09
CuO_6@MoS_2	4.80	5.02	6.53	6.47	6.86	10.10
ZnO_6@MoS_2	4.80	5.01	6.53	6.47	6.88	10.90

Table S20. The bader charge of OH^* absorbed on transition metal atom (TM) co-doped with six oxygen atoms in 2H phase MoS_2, including nearest neighbor Mo atoms (Mo^1), other Mo atoms (Mo^2), nearest neighbor S atoms (S^1), other S atoms (S^2), O on the same side of OH adsorbent (O^1), O on the opposite side of OH^* adsorbent (O^2), O in OH^* adsorbent (O^3), H in OH^* adsorbent (H^0) and transition metal atom (TM).

Material systems	Mo^1	Mo^2	S^1	S^2	O^1	O^2	O^3	H^0	TM
ScO_6@MoS_2	4.64	5.02	6.53	6.49	7.06	6.77	7.44	0.20	8.96
TiO_6@MoS_2	4.67	5.01	6.54	6.49	6.98	6.78	7.16	0.21	2.18
VO_6@MoS_2	4.73	5.00	6.51	6.49	6.83	6.85	6.99	0.23	3.44
CrO_6@MoS_2	4.66	5.03	6.52	6.48	6.92	6.79	7.08	0.22	4.40
MnO_6@MoS_2	4.65	5.02	6.53	6.49	6.93	6.78	6.98	0.36	5.54
FeO_6@MoS_2	4.63	5.01	6.53	6.49	6.98	6.77	7.17	0.21	6.56
CoO_6@MoS_2	4.64	5.01	6.52	6.49	6.92	6.77	6.95	0.32	7.81
NiO_6@MoS_2	4.63	5.02	6.53	6.48	6.77	6.90	7.18	0.00	8.99
CuO_6@MoS_2	4.61	5.03	6.52	6.48	6.88	6.77	7.25	0.00	10.12
ZnO_6@MoS_2	4.59	5.04	6.53	6.47	6.94	6.80	7.39	0.00	10.75

Table S21. Values used for the entropy and zero-point energy corrections in determining the free energy of reactants, products, and intermediate species adsorbed on catalysts. For the adsorbates, the ΔZPE values are averaged over all transition metal atom doped in 2H phase MoS_2 catalyst systems since they have rather close value.

Species	TS (eV)(298K)	ZPE (eV)
H^*	0	0.17
O^*	0	0.07
OH^*	0	0.33
OOH^*	0	0.43
H_2(g)	0.41	0.27
H_2O(g)	0.58	0.57

Table S22. Adsorption free energies of OH^*, O^*, OOH^* (eV) and theoretical overpotential for OER (η^{OER}, V vs RHE) on transition metal atom co-doped with six oxygen atoms in 2H phase MoS_2. The catalytic performance better than or comparable to IrO_2 is marked with red.

Material systems	ΔG_{OH^*}	ΔG_{O^*}	ΔG_{OOH^*}	η^{OER}
YO_6@MoS_2	1.05	4.68	4.76	2.40
ZrO_6@MoS_2	2.17	4.45	4.99	1.05
NbO_6@MoS_2	2.06	2.62	5.59	1.73
RuO_6@MoS_2	1.79	3.58	4.63	0.56
RhO_6@MoS_2	1.64	3.56	4.31	0.69
PdO_6@MoS_2	2.58	4.64	5.13	1.35
AgO_6@MoS_2	2.57	4.65	5.25	1.34
CdO_6@MoS_2	1.33	4.22	4.35	1.65
IrO_6@MoS_2	2.25	3.52	4.46	1.02
PtO_6@MoS_2	2.06	3.86	5.12	0.83

Table S23. Adsorption free energies of OH^*, O^*, OOH^* (eV) and theoretical overpotential for OER (η^{OER}, V vs RHE) on transition metal atom co-doped with six

oxygen atoms and transition metal atom doped in 2H phase MoS_2, respectively. The catalytic performance better than or comparable to IrO_2 is marked with red.

Species	ΔG_{OH}^*	ΔG_O^*	ΔG_{OOH}^*	η^{OER}
Sc@MoS_2	1.21	1.68	4.63	1.72
Ti@MoS_2	1.25	1.71	4.63	1.69
V@MoS_2	1.19	1.70	4.56	1.63
Cr@MoS_2	2.36	1.63	4.79	1.93
Mn@MoS_2	1.84	1.57	3.59	0.79
Fe@MoS_2	1.62	1.50	3.56	0.83
Co@MoS_2	0.80	1.48	4.30	1.59
Ni@MoS_2	0.35	1.47	3.84	1.14
Cu@MoS_2	0.64	1.15	4.12	1.74
Zn@MoS_2	0.89	1.39	4.35	1.73
MoS_2	2.65	1.77	4.92	1.92
ScO_6@MoS_2	1.19	3.94	4.38	1.52
TiO_6@MoS_2	1.67	2.88	5.07	0.96
VO_6@MoS_2	2.76	2.23	5.04	1.58
CrO_6@MoS_2	2.24	2.51	4.41	1.01
MnO_6@MoS_2	1.34	2.43	4.20	0.54
FeO_6@MoS_2	1.16	2.66	4.36	0.48
CoO_6@MoS_2	1.53	2.85	4.43	0.36
NiO_6@MoS_2	1.83	3.37	4.70	0.60
CuO_6@MoS_2	2.14	4.75	5.19	1.39
ZnO_6@MoS_2	1.33	4.41	4.40	1.85

Table S24. The bader charge of transition metal atom (TM) co-doped with six oxygen atoms in 2H phase MoS_2, and the bader charge of transition metal atom (TM) doped in 2H phase MoS_2, including nearest neighbor Mo atoms (Mo^1), other Mo atoms (Mo^2), nearest neighbor S atoms (S^1), other S atoms (S^2), O atom (O^0) and transition metal atom (TM).

Material systems	Mo^1	Mo^2	S^1	S^2	O^0	TM
Sc@MoS_2	5.01	5.04	6.59	6.48	/	9.51
Ti@MoS_2	5.02	5.05	6.57	6.47	/	2.70
V@MoS_2	5.03	5.05	6.53	6.47	/	3.86

Cr@MoS_2	5.00	5.06	6.49	6.47	/	5.11
Mn@MoS_2	4.97	5.00	6.47	6.50	/	6.26
Fe@MoS_2	4.97	4.96	6.46	6.52	/	7.33
Co@MoS_2	5.01	5.05	6.38	6.48	/	8.53
Ni@MoS_2	4.95	5.01	6.45	6.49	/	9.46
Cu@MoS_2	4.99	4.97	6.44	6.51	/	10.43
Zn@MoS_2	4.96	5.01	6.52	6.49	/	11.19
MoS_2	5.04	5.05	6.48	6.47	/	5.07
ScO_6@MoS_2	4.87	5.02	6.49	6.48	6.92	9.17
TiO_6@MoS_2	4.90	5.02	6.49	6.47	6.88	2.27
VO_6@MoS_2	4.85	5.01	6.50	6.48	6.86	3.41
CrO_6@MoS_2	4.85	5.00	6.51	6.48	6.85	4.54
MnO_6@MoS_2	4.88	5.01	6.50	6.47	6.85	5.67
FeO_6@MoS_2	4.87	5.01	6.48	6.47	6.86	6.74
CoO_6@MoS_2	4.89	5.02	6.48	6.47	6.83	7.86
NiO_6@MoS_2	4.84	5.01	6.50	6.47	6.84	9.09
CuO_6@MoS_2	4.80	5.02	6.53	6.47	6.86	10.10
ZnO_6@MoS_2	4.80	5.01	6.53	6.47	6.88	10.90

Table S25. The bond length of transition metal atom (TM) co-doped with six oxygen atoms in 2H phase MoS_2, and the bond length of transition metal atom (TM) doped in 2H phase MoS_2, including nearest neighbor Mo atoms (Mo), nearest neighbor S atoms (S), O atom (O) and transition metal atom (TM).

Material systems	Mo-S	Mo-O	TM-O	TM-S
Sc@MoS_2	2.40	/	/	2.52
Ti@MoS_2	2.40	/	/	2.43
V@MoS_2	2.41	/	/	2.36
Cr@MoS_2	2.41	/	/	2.32
Mn@MoS_2	2.42	/	/	2.30
Fe@MoS_2	2.42	/	/	2.30
Co@MoS_2	2.42	/	/	2.29
Ni@MoS_2	2.40	/	/	2.42
Cu@MoS_2	2.42	/	/	2.43
Zn@MoS_2	2.40	/	/	2.51
MoS_2	2.41	/	/	/
ScO_6@MoS_2	2.42	2.04	2.21	/
TiO_6@MoS_2	2.43	2.06	2.09	/
VO_6@MoS_2	2.44	2.07	2.01	/

CrO_6@MoS_2	2.44	2.08	1.99	/
MnO_6@MoS_2	2.43	2.06	1.99	/
FeO_6@MoS_2	2.43	2.03	2.17	/
CoO_6@MoS_2	2.43	2.03	2.16	/
NiO_6@MoS_2	2.42	2.03	1.97	/
CuO_6@MoS_2	2.42	2.04	1.98	/
ZnO_6@MoS_2	2.42	2.08	1.95	/

Table S26. The adsorption energy of CO, OH and OH+H on 3d-TMO_6@MoS_2.

Material systems	ΔE_{OH}	ΔE_{OH+H}	ΔE_{CO}
ScO_6@MoS_2	-2.36	0.64	0.30
TiO_6@MoS_2	-1.89	2.11	0.30
VO_6@MoS_2	-0.80	1.30	0.30
CrO_6@MoS_2	-1.32	1.65	0.30
MnO_6@MoS_2	-2.21	0.92	0.30
FeO_6@MoS_2	-2.40	0.49	0.29
CoO_6@MoS_2	-2.03	0.84	0.29
NiO_6@MoS_2	-1.28	0.96	-0.01
CuO_6@MoS_2	-1.42	-0.49	0.28
ZnO_6@MoS_2	-2.23	-0.85	0.28

Table S27. Adsorption free energies of OH^*, O^*, OOH^* (eV) and theoretical overpotential for OER (η^{OER}, V vs RHE) on transition metal atom co-doped with six oxygen atoms in 2H phase MoS_2 with different defect structures (S-vacancy, Mo-vacancy, S-edge, Mo-edge). The catalytic performance better than or comparable to IrO_2 is marked with red.

Material systems	ΔG_{OH}^*	ΔG_O^*	ΔG_{OOH}^*	η^{OER}
MoS_2	2.65	1.77	4.92	1.92
S-vacancy@MoS_2	-0.17	-1.56	1.50	2.19
S-edge@MoS_2	0.33	1.19	3.54	1.12
Mo-vacancy @MoS_2	1.14	1.58	3.18	0.51
Mo-edge @MoS_2	-2.28	-2.57	-4.06	7.75
CuO_6-S-vacancy@MoS_2	-1.96	-1.82	0.84	2.85

CuO_6-S-edge@MoS_2	-1.10	-0.58	2.27	1.62
CuO_6-Mo-vacancy @MoS_2	0.47	1.61	3.98	1.14
CuO_6-Mo-edge @MoS_2	-2.09	-2.15	1.21	2.48
FeO_6-S-vacancy@MoS_2	-2.03	-2.01	0.87	2.82
FeO_6-S-edge@MoS_2	0.68	1.56	3.94	1.16
FeO_6-Mo-vacancy @MoS_2	0.99	1.61	4.07	1.22
FeO_6-Mo-edge @MoS_2	-1.63	-1.76	1.53	2.16

Table S28. OH^* adsorption free energies of tetra-coordinated structure (TMO_3-OH) and hexa-coordinated structure (TMO_6-OH) of TM (TM=Co and Fe) co-doped six oxygen atoms in 2H phase MoS_2 during OER reaction. The more thermodynamically stable coordination structure is marked with red.

Material systems	ΔE(TMO_3-OH)	ΔE(TMO_6-OH)
ScO_6@MoS_2	1.19	2.80
TiO_6@MoS_2	1.67	2.68
VO_6@MoS_2	2.76	2.81
CrO_6@MoS_2	2.24	2.84
MnO_6@MoS_2	1.34	2.20
FeO_6@MoS_2	1.16	2.68
CoO_6@MoS_2	1.53	2.43
NiO_6@MoS_2	1.83	2.34
CuO_6@MoS_2	2.14	2.64
ZnO_6@MoS_2	1.33	2.45

References

1. Y. Zhou, J. Zhang, E. Song, J. Lin, J. Zhou, K. Suenaga, W. Zhou, Z. Liu, J. Liu, J. Lou and H. J. Fan, *Nat. Commun.*, 2020, **11**, 2253.
2. Y. Zhou, W. Hao, X. Zhao, J. Zhou, H. Yu, B. Lin, Z. Liu, S. J. Pennycook, S. Li and H. J. Fan, *Adv. Mater.*, 2021, 2100537.
3. Y. Wang, R. Zhang, X. Zhao, Y. Min and C. Liu, *ISIJ International*, 2020, **60**, 220-225.
4. D. Scarano, A. Zecchina, S. Bordiga, F. Geobaldo, G. Spoto, G. Petrini, G. Leofanti, M. Padovan and G. Tozzola, *Journal of the Chemical Society, Faraday Transactions*, 1993, **89**, 4123-4130.
5. K. Hedenstedt, J. Bäckström and E. Ahlberg, *J. Electrochem. Soc.*, 2017, **164**, H621-H627.
6. T. Baruah, R. R. Zope and M. R. Pederson, *Physical Review A*, 2004, **69**.
7. X. Pang, H. Bai, H. Zhao, W. Fan and W. Shi, *ACS Catalysis*, 2022, **12**, 1545-1557.
8. Y. Wang, W. M. Sun, X. F. Ling, X. K. Shi, L. L. Li, Y. D. Deng, C. H. An and X. P. Han, *Chem.-Eur. J.*, DOI: 10.1002/chem.201904238, 8.
9. Z. Y. Zhao, F. L. Li, Q. Shao, X. Q. Huang and J. P. Lang, *Adv. Mater. Interfaces*, 2019, **6**, 9.
10. B. S. Tang, Z. G. Yu, H. L. Seng, N. D. Zhang, X. X. Liu, Y. W. Zhang, W. F. Yang and H. Gong, *Nanoscale*, 2018, **10**, 20113-20119.
11. Q. Z. Xiong, Y. Wang, P. F. Liu, L. R. Zheng, G. Z. Wang, H. G. Yang, P. K. Wong, H. M. Zhang and H. J. Zhao, *Adv. Mater.*, 2018, **30**, 7.
12. Q. Xiong, X. Zhang, H. J. Wang, G. Q. Liu, G. Z. Wang, H. M. Zhang and H. J. Zhao, *Chem. Commun.*, 2018, **54**, 3859-3862.
13. H. Lee, J. Y. Kim, S. Lee, J. A. Hong, N. Kim, J. Baik and Y. J. Hwang, *Sci Rep*, 2018, **8**, 8.
14. R. P. Forslund, W. G. Hardin, X. Rong, A. M. Abakumov, D. Filimonov, C. T. Alexander, J. T. Mefford, H. Iyer, A. M. Kolpak, K. P. Johnston and K. J. Stevenson, *Nat. Commun.*, 2018, **9**, 11.
15. D. W. Wang, Q. Li, C. Han, Q. Q. Lu, Z. C. Xing and X. R. Yang, *Nat. Commun.*, 2019, **10**, 12.
16. K. Fan, H. Chen, Y. F. Ji, H. Huang, P. M. Claesson, Q. Daniel, B. Philippe, H. Rensmo, F. S. Li, Y. Luo and L. C. Sun, *Nat. Commun.*, 2016, **7**, 9.
17. Z. Y. Lu, L. Qian, Y. Tian, Y. P. Li, X. M. Sun and X. Duan, *Chem. Commun.*, 2016, **52**, 908-911.
18. J. Jiang, F. F. Sun, S. Zhou, W. Hu, H. Zhang, J. C. Dong, Z. Jiang, J. J. Zhao, J. F. Li, W. S. Yan and M. Wang, *Nat. Commun.*, 2018, **9**, 12.
19. S. Jaskaniec, C. Hobbs, A. Seral-Ascaso, J. Coelho, M. P. Browne, D. Tyndall, T. Sasaki and V. Nicolosi, *Sci Rep*, 2018, **8**, 8.
20. L. Zhou, C. Zhang, Y. Q. Zhang, Z. H. Li and M. F. Shao, *Adv. Funct. Mater.*, DOI: 10.1002/adfm.202009743, 9.
21. Y. Wang, W. M. Sun, X. F. Ling, X. K. Shi, L. L. Li, Y. D. Deng, C. H. An and X. P. Han, *Chem.-Eur. J.*, 2020, **26**, 4097-4103.